Agricultural and Forest Meteorology 379 (2026) 111056

Contents lists available at ScienceDirect

Agricultural and Forest Meteorology

journal homepage: www.elsevier.com/locate/agrformet

Temperature and photoperiod interactions influence the cessation of wood growth in three temperate and boreal conifers

Jianhong Lin [a,*], Cyrille B.K. Rathgeber [b], Patrick Fonti [c], Sergio Rossi [d], Henri Cuny [e], Edurne Martinez del Castillo [f], Katarina Čufar [g], J. Julio Camarero [h], Alessio Giovannelli [i], Harri Mäkinen [j], Peter Prislan [k], Walter Oberhuber [l], Hanuš Vavrčík [m], Jianguo Huang [n], Andreas Gruber [l], Vladimír Gryc [m], Václav Treml [o], Martin de Luis [p], Jožica Gričar [k], Nicolas Delpierre [a,q]

[a] Université Paris-Saclay, CNRS, AgroParisTech, Ecologie Société Evolution, Gif-sur-Yvette 91190, France
[b] Université de Lorraine, AgroParisTech, INRAE, SILVA, Nancy 54000, France
[c] Swiss Federal Institute for Forest, Snow and Landscape Research WSL, Birmensdorf, Switzerland
[d] Université du Québec à Chicoutimi, 555, Boulevard de l'Université, Chicoutimi, QC G7H 2B1, Canada
[e] IGN, Service de l'Information Forestière, Champigneulles 54250, France
[f] Geography Department, Johannes Gutenberg University Mainz, Germany
[g] Biotechnical Faculty, University of Ljubljana, Jamnikarjeva 101, Ljubljana 1000, Slovenia
[h] Instituto Pirenaico de Ecología (IPE-CSIC), Zaragoza 50192, Spain
[i] National Research Council – Research Institute on Terrestrial Ecosystems (CNR-IRET), Via Madonna del Piano, 10, Sesto Fiorentino 50019, Italy
[j] Natural Resources Institute Finland, Latokartanonkaari 9, Helsinki 00790, Finland
[k] Slovenian Forestry Institute, Večna pot 2, Ljubljana 1000, Slovenia
[l] Department of Botany, University of Innsbruck, Sternwartestraße 15, Innsbruck 6020, Austria
[m] Faculty of Forestry and Wood Technology, Department of Wood Science and Technology, Mendel University in Brno, Zemědělská 1, Brno 613 00, Czech Republic
[n] State Key Laboratory for Vegetation Structure, Function and Construction, College of Life Sciences, Zhejiang University, Hangzhou 310058, China
[o] Department of Physical Geography and Geoecology, Faculty of Science, Charles University, Albertov 6, Prague 12800, Czech Republic
[p] Departamento de Geografía y Ordenación del Territorio - IUCA, Universidad de Zaragoza, Spain
[q] Institut Universitaire de France (IUF), Paris 75005, France

ARTICLE INFO

Keywords:
Cambium phenology
Ecophysiological models
Xylem formation
Climate change
Global warming
Northern hemisphere forests

ABSTRACT

Cambium phenology is a crucial process in wood production and carbon sequestration of forest ecosystems. Although cambium phenology has been widely studied, research specifically focusing on the cessation of wood formation remains limited. To better understand the influence of environmental and intrinsic factors on the cessation of wood formation, we built and compared three ecophysiological models (*temperature sum* model, *photoperiod-influenced temperature sum* model and *soil moisture- and photoperiod-influenced temperature sum* model) in their ability to predict the date of cessation of xylem cell enlargement (cE) in three major Northern Hemisphere conifer species (Black spruce, Norway spruce and Scots pine). We developed these models based on xylogenesis data collected for 130 site-years across Europe and Canada. Our results demonstrate that the *photoperiod-influenced temperature sum* model is well-supported by data across all conifer species, with a RMSE of 9.2 days, suggesting that both temperature and photoperiod are critical drivers of wood growth cessation. However, incorporating soil moisture effects does not improve model performance. Our model effectively captures the inter-site variability in cE across a wide environmental gradient, with a fair model efficiency (ME = 0.51 ± 0.22), but performed less well for annual anomalies (ME = 0.10 ± 0.09). Additionally, we found that the total ring cell number also affected prediction accuracy. Using this model, we reconstructed historical trends in cE over the past six decades and found a trend to delayed cessation dates. This delay varied geographically, with slower shifts at higher latitudes and elevations, likely due to constrained cambial responses and conservative growth strategies in colder regions. Our model framework offers a simple yet accurate approach for predicting

* Corresponding author.
E-mail address: jianhong.lin@universite-paris-saclay.fr (J. Lin).

https://doi.org/10.1016/j.agrformet.2026.111056
Received 30 June 2025; Received in revised form 9 December 2025; Accepted 29 January 2026
Available online 4 February 2026

wood growth cessation at large spatial scales, providing a basis for integrating cambium phenology into land surface models and forest productivity assessments.

1. Introduction

Cambium phenology is crucial for plant functioning and ecosystem services (Cabon et al., 2020; Chen et al., 2022; Huang et al., 2023; Rossi et al., 2011). Changes in cambium phenology, such as the onset, cessation, or duration of wood formation, can significantly impact the amount of carbon sequestrated by trees under changing climate conditions (Chen et al., 2022; Delpierre et al., 2019; Eckes-Shephard et al., 2022). Despite its importance, cambium phenology has been relatively understudied compared to leaf phenology (Delpierre et al., 2016; Dox et al., 2022). Similarly to the autumnal phases of leaf phenology, the cessation of wood formation remains less studied than its onset in spring, probably due to the complex interplay between environmental and intrinsic factors influencing it (Cuny et al., 2019; Dox et al., 2020; Rossi et al., 2016). Furthermore, tracking the cessation of wood formation is inherently more challenging than its beginning, as it involves subtler, slower, and less visible processes (Rathgeber et al., 2016). While ecophysiological models exist for predicting the onset of wood formation (Delpierre et al., 2019), models for its cessation are notably lacking. This represents a critical research gap, as the timing of cessation of wood formation is rarely represented in terrestrial ecosystem models (TEMs), although influencing the simulated productivity (Delpierre et al., 2016; Friend et al. 2019). In this context, developing robust ecophysiological models for simulating the seasonal cessation of wood formation is essential.

In the process of wood formation, the cessation of xylem radial growth typically occurs in summer or earlier under unfavourable temperature or water deficit conditions (Saderi et al. 2019). This process follows a sequential pattern: first, cambium cell division ceases, followed by the cessation of xylem cell enlargement, with a time lag varying among species (Rossi et al., 2006b), marked by the end of radial expansion of xylem cells. Several weeks later, the cessation of cell wall thickening marks the completion of wood formation and the end of carbon sequestration (Cuny et al., 2015).

The seasonality of wood formation results from a complex interplay between environmental and intrinsic factors (Aloni, 2013; Delpierre et al., 2016; Rossi et al., 2016). Temperature, a key environmental factor, directly influences wood formation by affecting cell structure (Cuny and Rathgeber, 2016; Friend et al., 2022; Rathgeber et al., 2016) and regulating processes such as cambial cell division, hormones metabolism and activity (Rathgeber et al., 2016; Schrader et al., 2003). Manipulative experiments show that locally-cooled stem sections stop cambial cell division earlier than non-cooled sections, confirming that low temperatures induce cambial dormancy (Begum et al., 2016; Begum et al., 2018; Gričar et al., 2006). Beyond temperature, soil moisture and photoperiod also influence cambium phenology. Reduced soil water availability can halt cambial activity and xylem cell enlargement (Cabon et al., 2020; Gričar and Čufar, 2008; Traversari et al., 2018), while photoperiod regulates peak growth rates and influences the cessation of wood formation in temperate and boreal forests (Cuny et al., 2015; Jackson, 2009; Rossi et al., 2006c). In addition to environmental influences, ontogenetic factors modulate cambium phenology, with younger and taller trees exhibiting longer periods of xylogenesis (Rathgeber et al., 2011a; Rossi et al., 2008; Zeng et al., 2017). Moreover, the onset of cambial activity determines the number of radial cells produced, which in turn influences the timing of the cessation of wood formation (Deslauriers et al., 2008; Gričar et al., 2005; Lupi et al., 2010; Rossi et al., 2012). In this context, disentangling the roles of environmental and tree internal factors is critical for developing robust predictive models of wood formation cessation.

Existing process based wood growth models can simulate xylem growth cessation (Cabon et al., 2020; Schiestl-Aalto et al., 2015; Vaganov et al., 2006), but they generally rely on bottom-up, cell-level frameworks and focus on intra-annual dynamics. Despite their mechanistic detail, these models often perform poorly in capturing growth cessation (e.g., the Vaganov–Shashkin model (Buttò et al., 2020; Tumajer et al., 2021)). Furthermore, the validation of such models has typically been restricted to narrow temporal and spatial scales (Cabon et al., 2020; Schiestl-Aalto et al., 2015). Similarly, statistical models of cambium phenology are often limited to case studies. A key example is the temperature-threshold model developed by Rossi et al. (2011), which, despite projecting delayed cessation of cell-wall thickening under warming, was calibrated using only a seven-year black spruce dataset and its applicability was restricted to a single species and region. These limitations underscore the urgent need for ecophysiological models capable of integrating multiple environmental drivers to robustly simulate wood formation cessation across broader geographic gradients, extended time periods, and diverse species.

Here we developed three ecophysiological models to predict the cessation of xylem cell enlargement in three conifer species (*Pinus sylvestris, Picea abies* and *Picea mariana*) across Europe and Canada. The models were parameterized and evaluated using direct observations of the date of cessation of xylem cell enlargement from the GloboXylo database. We tested the hypotheses that (a) all ecophysiological models can effectively capture the cessation of xylem cell enlargement (cE in the following), with the most accurate prediction coming from the model incorporating temperature, photoperiod, and soil moisture as environmental drivers; (b) tree characteristics, including total ring cell number (RCN), age, height, and diameter at breast height (DBH), also influence cE; and (c) retrospective model simulations would reveal a trend toward later cessation dates of xylem cell enlargement over the past six decades, but the magnitude of the delay differs by region. To test these hypotheses, we aimed to: (1) assess whether the interannual and inter-site variability of cE could be explained by (a) temperature alone, (b) the combined effects of temperature and photoperiod, or (c) the combined effects of temperature, photoperiod, and soil moisture; (2) evaluate the influence of tree characteristics (e.g., RCN, age, height, and DBH) on cE; and (3) identify long-term trends in cE and quantify the spatial variability in the magnitude of these trends.

2. Material and methods

2.1. Study sites

We used wood formation data from 34 sites across the Northern Hemisphere, covering a broad range of temperature and photoperiod conditions (40.0°N to 67.5°N, 79.2°W to 26.4°E) and elevations from 30 m to 2,156 m asl (Fig. 1, Supporting Information Table 1). These data were collated in the GloboXylo database (https://appgeodb-preprod.nancy.inrae.fr/globoxylo/en/) and include wood formation and meteorological records collected by multiple research teams from 2002 to 2013 (Table 1, Supplementary Table 1). For this work, we focused on three coniferous species well-represented in the database, namely Scots pine (*Pinus sylvestris* L.), Norway spruce (*Picea abies* Karst.) and black spruce (*Picea mariana* Mill.). In total, we analyzed 718 observations of the date of the cessation of xylem cell enlargement across 130 site-years. All sampled trees were dominant individuals, with an average (± SD) age of 119 ± 56 years, a diameter at breast height (DBH) of 31.4 ± 14.6 cm, and a tree height of 20.0 ± 7.8 m (Supplementary Table 1).

2.2. Wood formation data

To observe wood formation phenology, 5 ± 2 trees were selected per study site and sampled every 1 or 2 weeks from May to October during 2002-2013, depending on local climate conditions. Microcore collection and processing followed established protocols (Prislan et al., 2022; Rathgeber et al., 2011b; Rossi et al., 2006a; Rossi et al., 2006b). At least three radial files were examined per tree. In this work we focused on the cessation of xylem cell enlargement (cE). cE was defined as the day of year (DoY) when less than 50% of the observed radial files contained one (or more) enlarging xylem cell, characterized by a wide lumen and thin primary walls (Rathgeber et al., 2011b). Observations from different research teams were systematically verified, standardized, and analysed using the R package CAVIAR (Rathgeber et al., 2011b, 2018), which applies logistic regressions and visualization tools to estimate the timing of key xylogenesis phases, such as the cessation of xylem cell enlargement.

2.3. Temperature and photoperiod data

Temperature data were monitored at the study sites (Fig. 1). However, some temperature records from local weather stations contained missing values. To fill these gaps, we used the EWEMBI gridded meteorological dataset (grid resolution = 0.5°, http://doi.org/10.5880/pik.2019.004, Frieler et al., 2017), and established linear regressions between the local observations and corresponding EWEMBI values. The correlation between overlapping local and EWEMBI temperature time series ranged from 0.95 to 0.99, ensuring high consistency. Day length was calculated daily as a function of latitude, using R package insol (Corripio, 2019). Soil moisture data (m^3 m^{-3}) was obtained from ERA5-Land reanalysis dataset provided by the European Center for Medium-Range Weather Forecast, with a grid resolution of 0.25° (Hersbach, 2023). For this study, we used soil moisture data from a depth range of 0–289 cm.

2.4. Model description

We designed and evaluated three ecophysiological models to predict cE in the three conifer species of interest (Table 2). The first model assumes that cumulative temperature is the main driver of cE, based on its strong correlation with xylem formation timing across climate gradients (Rossi et al., 2016) and that low temperature can induce the cessation of cambium activity (Begum et al., 2018; Gričar et al., 2006). The second model adds photoperiod as a co-regulator, reflecting its established role in growth cessation. This formulation parallels prior models for autumnal leaf senescence (Delpierre et al., 2009). The third model extends the second by incorporating soil moisture, following Wu et al. (2022), to simulate earlier cE under drought conditions. This addition accounts for the role of water availability in limiting turgor-driven cell expansion.

2.4.1. Temperature sum (Ts) model

To represent the influence of decreasing temperatures on cE, we built upon the model of Delpierre et al. (2009), who proposed a model of leaf senescence based on cooling degree-days.

In this model (*Ts* model in the following), we assume that cE occurs when temperature accumulation (below a specific threshold) reaches a critical value.

The model is based on a temperature-dependent accumulation rate *Rc(t)*, defined as:

$$Rc(t) = \begin{cases} 0, & T(t) > T_b \\ (T_b - T(t))^x, & T(t) \le T_b \end{cases} \quad (1)$$

where *T(t)* is the daily mean air temperature on day *t*, T_b is the maximum temperature threshold below which temperature influences cE (°C), *x* is a dummy parameter that can take values (0, 1, 2) to represent absent, proportional, or more-than-proportional temperature effects (Delpierre et al., 2009). Higher (up to three) and continuous (non-discrete) values of the *x* were tested in preliminary simulations, but they did not improve the model's fit.

The temperature accumulation *S(t)* is computed as the cumulative sum of *Rc* from a defined starting date *Dstart* until day *t*:

$$S(t) = \sum_{Dstart}^{t} Rc \quad (2)$$

The day of wood formation cessation, cE, is then identified as the first day *t* when the accumulated temperature *S(t)* reaches the required temperature accumulation *Ycrit* (in degree-days):

$$cE = (t) \text{ such that } S(t) \ge Ycrit \quad (3)$$

2.4.2. Photoperiod-influenced temperature sum (PiTs) model

In the photoperiod-influenced temperature sum (*PiTs*) model, we also assumed that cE occurs when a given accumulation of temperature is reached. However, unlike the *Ts* model, the rate of temperature accumulation is modified by night length. This adjustment accounts for the role of photoperiod in influencing the cessation of xylem enlargement (Mu et al., 2023). The temperature accumulation rate *Rc(t)* is calculated as follows:

$$Rc(t) = \begin{cases} 0, & T(t) > T_b \\ (T_b - T(t))^x \times f[P(t)]^y, & T(t) \le T_b \end{cases} \quad (4)$$

where *P(t)* is the night length on the day *t*, *f[P(t)]* is a photoperiod

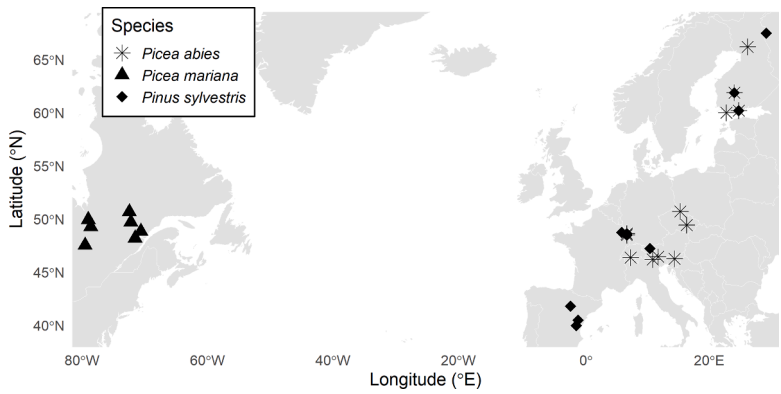

Fig. 1. Distribution of the study sites.

function defined as:

$$f[P(t)] = P(t) - NLmin \quad (5)$$

where *NLmin* is the minimum night length at each site (i.e. occurring at summer solstice). Since our dataset span a wide latitudinal gradient, we accounted for site-to-site variability in absolute night length by considering relative night length, subtracting the minimum night length at each site. In Eq. (4), the dummy parameter *y* may take discrete values (0, 1, 2) to allow for any absent, proportional, or more than proportional effects of photoperiod (Delpierre et al., 2009). Preliminary tests with higher (up to three) and continuous (non-discrete) values of the *y* did not improve model performance.

2.4.3. Soil moisture- and photoperiod-influenced temperature sum (SMPiTs) model

Building upon the *PiTs* model, we developed a third variant, the soil moisture- and photoperiod-influenced temperature sum model (*SMPiTs* model), to account for the influence of soil moisture on cE. Consistent with assumptions of the two other models, we posit that cE occurs when the accumulated temperature surpasses a critical threshold *Ycrit*. However, we further hypothesized that *Ycrit* is modulated by pre-season soil moisture (PreSM, in $m^3\ m^{-3}$) considered during the month preceding the average cE date across all populations of a given tree species. This approach draws on the methodology proposed by Wu et al. (2022), which examined the effects of soil moisture on leaf senescence. In *SMPiTs*, we calculate *Ycrit* as follows:

$$Ycrit = a + b \times PreSM + c \times PreSM^2 \quad (6)$$

where *a, b, c* are model parameters quantifying the effect of soil moisture on *Ycrit*.

The calculation of *Rc* remains consistent with the *PiTs* model (Eqs. (4) and (5)). cE is determined using Eqs. (2), (3), and *Ycrit* from Eq. (6).

2.5. Model calibration and validation

The cE data observed at the tree scale were randomly split into calibration (70%) and validation (30%) subsets, with calibration performed at the site-year level. To ensure comparability, we verified that the distributions of the calibration and validation subsets were statistically similar using the Wilcoxon rank-sum test ($p>0.50$). To address potential variability in model fitting and parameter estimation arising from the specific calibration subset chosen, the calibration procedure was repeated 100 times, each using a new random split of the data at the site-year level (Delpierre et al. 2019). Model evaluation results reported below are based on the validation subsets (i.e. independent from calibration data).

Model parameters were fitted using the '*optim*' function in R software (R Core Team, 2023). The lower and upper bounds used in the parameter fitting procedure are provided in Supplementary Table 2.

Model performance was evaluated using the root mean square error (RMSE), model efficiency (ME), and the corrected Akaike information criterion (AICc). Among the three metrics, AICc is primarily used to select the best-fitting model, as it balances model accuracy and parsimony. The model with the lowest AICc is considered to be the best supported by the data. Model comparisons are based on ΔAICc, where a difference of less than 2 indicates that models are equivalent (Burnham and Anderson, 2002).

Table 2
Overview of the tested models and their parameters. T_b is the maximum temperature at which the processes leading to the cessation of cell enlargement are considered to be effective (°C). The dummy parameter *x, y* may take any of the (0, 1, 2) discrete values, to allow for any absent/proportional/more than proportional effects of temperature to be included (Delpierre et al., 2009). *Ycrit* is the requirement of low temperature accumulation (in degree-days). *Dstart* is the start date of temperature accumulation (DoY). *a, b, c* are the parameters evaluating the effect of soil moisture on *Ycrit*.

Model name	Type	Environmental variables	Fitted parameters (Number of parameters)	Equations
Ts	Temperature sum	Temperature	T_b, *x, Ycrit, Dstart* (4)	(1), (2), (3)
PiTs	Photoperiod-influenced temperature sum	Temperature, photoperiod	T_b, *x, y, Ycrit, Dstart* (5)	(2), (3), (4), (5)
SMPiTs	Soil moisture and photoperiod-influenced temperature sum	Temperature, photoperiod, soil moisture	T_b, *x, y, a, b, c, Dstart* (7)	(2), (3), (4), (5), (6)

2.6. Evaluating the model ability to simulate inter-site and interannual variability

We assessed the model ability to simulate the inter-site and interannual variability of cE. For this, 1) we compared the predicted and observed cE, averaged at the scale of the site; and 2) we compared the annual observed and simulated cE anomalies, calculated as the difference between the cE data at the site-year scale and the site average cE date, which was established over the observation period.

2.7. Temporal changes of cE

To examine the spatial variability in the temporal changes of cE over the past six decades, we reconstructed the timing of cE from 1960 to 2023 using our modelling approach and temperature data sourced from ERA5-Land (gridded dataset, 0.1° resolution; Muñoz Sabater et al., 2024). We established linear regressions between the local observations and corresponding ERA5-Land values to remove biases in ERA5-Land data. The temporal changes of cE (in days $year^{-1}$) were calculated for each site. A linear model was then used to evaluate the effects of elevation and latitude on the temporal changes. Elevation and latitude data were standardized using z-scores prior to analysis.

2.8. The effect of ontogenetic factors and individual tree dimensions on cE

To assess the impact of tree "intrinsic factors" on cE, we analysed the relationships between tree characteristics (annual ring cell number (RCN), age, height, and diameter at breast height (DBH)) and our model residuals. Apart from RCN, which is at the tree level, all other intrinsic factors are site-level averages. The model residuals are calculated as the observed cE minus the predicted cE. We used the "*corrplot*" function from the R package corrplot (Wei and Simko, 2021) to visualize the Pearson correlations between tree characteristics and model residuals.

Table 1
Overview of cambium phenology data for three Northern Hemisphere conifer species. cE is the date (day of year, DoY) of the cessation of xylem cell enlargement. MAT refers to mean annual temperature, with standard deviation shown in parentheses.

Species	Number of sites	Year	cE (min/mean/max, DoY)	Elevation (min/median/max, m)	MAT (sd, °C)
Picea abies	19	2004-2005, 2007-2013	207/231/257	30/1350/2085	5.1 (2.4)
Picea mariana	7	2002-2010	196/214/233	271/342/611	0.9 (1.7)
Pinus sylvestris	13	2005-2011, 2013	221/248/277	60/430/1690	8.1 (3.0)

2.9. The effect of within-population variability of cE on prediction accuracy

We tested whether within-population variability in cE affects the model prediction accuracy. We quantified the model prediction accuracy with the RMSE, calculated for each site-year over the observed and predicted cE values for individual trees. (Note that our ecophysiological models predict one cE date for each site-year, but that cE can vary among trees observed in a given site-year.). Population variability in cE was represented by the standard deviation of cE across all trees within each site-year.

3. Results

3.1. Observations of the cessation of xylem cell enlargement

In our dataset, the observed date of cessation of xylem cell enlargement (cE) varied from 15 July (DoY196) for black spruce (*Picea mariana*) to 3 October (DoY 277) for Scots pine (*Pinus sylvestris*), spanning 81 days (Table 1). In general, black spruce was the earliest species to stop cell enlargement, on average on DoY 214 ± 9, followed by Norway spruce (*Picea abies*, DoY 231 ± 12, 2 weeks after) and Scots pine (DoY 248 ± 17, 4 weeks after). cE spanned 37 days for black spruce to 56 days for Scots pine (Table 1), reflecting the species-specific differences in data collection areas (larger for Scots pine and Norway spruce, lower for black spruce, Fig. 1).

3.2. Performance of the models

Among the three models considered (*Ts, PiTs, SMPiTs*), the *PiTs* model performed best for predicting cE in Norway spruce and black spruce, as indicated by the lowest AICc values and highest ME (Table 3). For Scots pine, the *PiTs* and *Ts* model yielded identical RMSE, with a lower AICc for the *Ts* model (of simpler structure). In the following, we will therefore consider *PiTs* as a reference model for species comparison. The *PiTs* model predicted cE with an average error of 9.2 ± 1.3 days for the three species (Fig. 2). A plot of the observed and simulated cE dates showed that *PiTs* model performed reasonably well at both the individual tree scale (grey dots in Fig. 2) and the site-year scale (colored points in Fig. 2), with most data points clustering near the 1:1 line. However, the *PiTs* model performance was lower for black spruce compared to Norway spruce and Scots pine despite a relatively low RMSE (8 days, Table 3). The *SMPiTs* model clearly performed worst for Norway spruce and Scots pine, with highest ΔAICc and RMSE (Table 3). In black spruce, although *SMPiTs* yielded a slightly lower RMSE than *PiTs*, its higher AICc suggests that the two models performed similarly

Table 3
Quality assessment of models for the cessation of xylem cell enlargement (cE). *Ts* model: The model which only considers the effect of temperature, *PiTs* model: The model considers the effect of temperature and photoperiod, *SMPiTs* model: The model considers the effect of temperature, photoperiod and soil moisture. Root mean square error (RMSE), model efficiency (ME), corrected Akaike Information Criterion (AICc) and ΔAICc are used to evaluate the model performance. ΔAICc represents the difference between the AICc of each model and the minimum AICc value among models for the same species. Bolded rows indicate the best-performing model (i.e., lowest AICc) for each species.

Species	Model	RMSE (days)	ME	AICc	ΔAICc
Picea abies	*Ts* model	9.7	0.30	1045.3	9.4
	***PiTs* model**	**9.2**	**0.37**	**1035.9**	**0**
	SMPiTs model	9.8	0.31	1054.9	19.0
Picea mariana	*Ts* model	8.4	0.12	680.2	5.4
	***PiTs* model**	**8.0**	**0.20**	**674.8**	**0**
	SMPiTs model	7.8	0.24	676.4	1.6
Pinus sylvestris	***Ts* model**	**10.5**	**0.60**	**441.8**	**0**
	PiTs model	10.5	0.60	445.0	3.2
	SMPiTs model	11.9	0.49	465.3	23.5

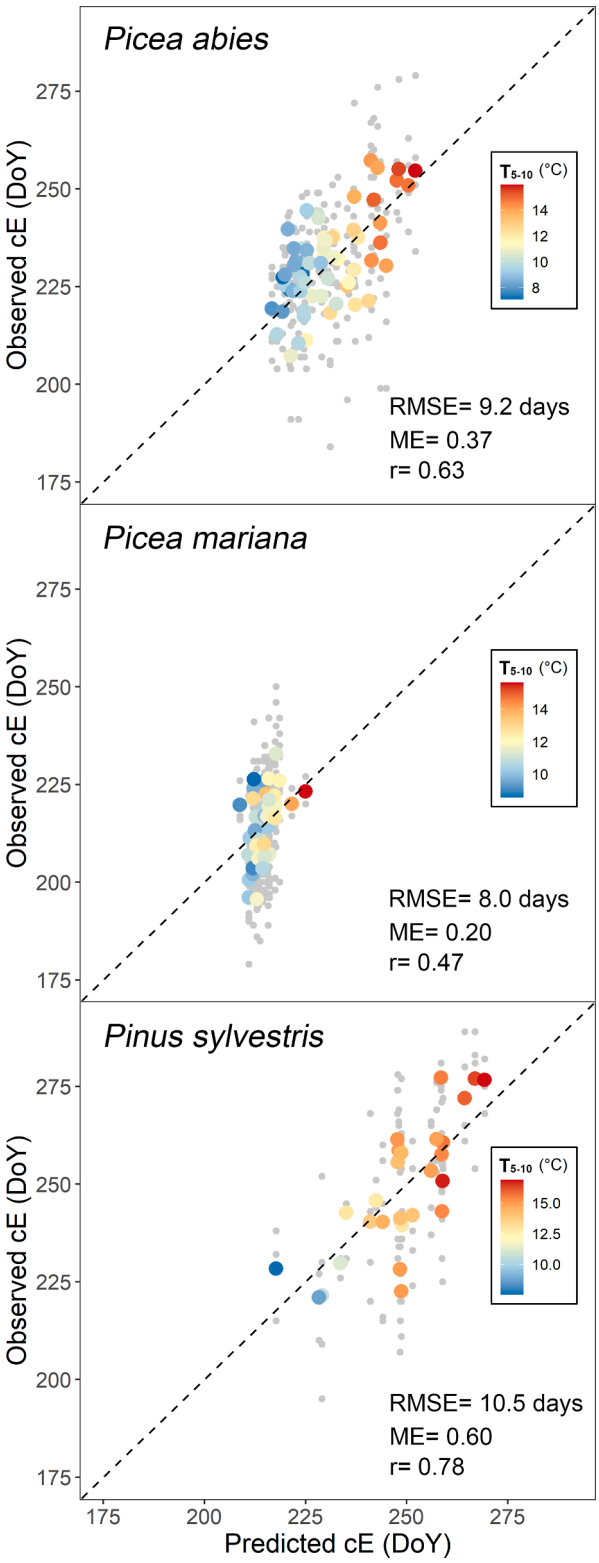

Fig. 2. Photoperiod-influenced low temperature sum (*PiTs*) model evaluation over validation data for three Northern Hemisphere coniferous tree species. The colored points establish the correspondence between the observed and predicted cessation of xylem cell enlargement (cE) at site-year scale. The point colors depict the mean temperature from May to October ($T_{5\text{-}10}$) for each site-year. The gray dots are the observed cE at the tree scale. The one-to-one relation is shown as a black dotted line. Root mean square error (RMSE), correlation coefficient (r) and model efficiency (ME) are used to illustrate the model performance.

Table 4
Parameters of *PiTs* model. T_b is the threshold of low temperature accumulation (°C), below which temperature can be accumulated. *Ycrit* is the requirement of low temperature accumulation. *Dstart* is the start date for low temperature accumulation (DoY). The dummy parameters *x* and *y* may take any of the {0, 1, 2} discrete values.

Species	T_b	*Ycrit*	*Dstart*	*x*	*y*
Picea abies	23.8	3075.8	200	2	1
Picea mariana	30.0	3105.7	190	2	1
Pinus sylvestris	23.7	2787.9	200	2	0

(ΔAICc < 2).

3.3. Parameters of the PiTs model

The fitted parameters of the PiTs model differed among species (Table 4). The upper temperature threshold (*Tb*) was comparable for Norway spruce and Scots pine (~23.8°C) but distinctly higher for black spruce (30.0°C). The temperature accumulation requirement (*Ycrit*) was highest for black spruce at 3105.7 degree-days, followed by Norway spruce at 3075.8 degree-days, and notably lower for Scots pine at 2787.9 degree-days. Regarding environmental drivers, both spruce species showed sensitivity to photoperiod (x = 2, y = 1), whereas Scots pine responded solely to temperature (x = 2, y = 0). The start date for temperature accumulation (*Dstart*), was similar across all species, with the earliest start in July, for black spruce on 9 July (DoY 190) and the latest start for both Norway spruce and Scots pine on 19 July (DoY 200). Parameter estimates varied across the 100 random calibration–validation splits, yet model performance remained highly consistent (Supplementary Fig. 1). Parameter distributions are shown in Supplementary Fig. 2.

3.4. Simulating the intersite and interannual variability of cE

The model's predictions for cE were effective at capturing inter-site variability, showcasing its strong ability to reflect differences among locations (Fig. 3a). The model achieved the lowest RMSE for black spruce (4.5 days), followed by Norway spruce (7.6 days), and the highest RMSE for Scots pine (8.3 days). This performance was further supported by the model efficiency (ME), with Norway spruce achieving ME of 0.38, black spruce at 0.39 and Scots pine at 0.76, indicating reasonable performance across different locations (Fig. 3). However, the model was less effective at capturing annual anomalies, especially for black spruce (Fig. 3b). Despite relatively low RMSE values, ME was low. For instance, Norway spruce had an RMSE of 6.7 days with a ME of 0.19, Scots pine showed an RMSE of 6.4 days but a ME of 0.10, and black spruce had an RMSE of 6.5 days with a ME of 0.02. This lower temporal predictive skill corresponds with the markedly higher temperature variability observed across sites compared to the limited year-to-year fluctuations within sites (Supplementary Fig. 3).

3.5. Geographic variability of the temporal changes of cE

Using the *PiTs* model, we reconstructed cE timing from 1960 to 2023 and quantified site-level linear trends. A significant delay in cE was detected across the past six decades, although the magnitude varied among species and regions (Fig. 4). Scots pine showed the largest delay (0.15 ± 0.09 days yr^{-1}), followed by Norway spruce (0.07 ± 0.05 days yr^{-1}) and black spruce (0.02 ± 0.01 days yr^{-1}). Variation among sites was greatest for Scots pine, consistent with its broad geographic range (Fig. 4a). Patterns in delay rate were further explained by elevation and latitude (Fig. 4b). For Norway spruce, both elevation and latitude had significant negative effects on the delay rate ($p < 0.001$), based on a multiple regression model including both predictors ($R^2_{adj} = 0.90$). For black spruce, latitude explained the variation in delay rate ($p < 0.1$), while elevation had no significant effect ($p > 0.1$; $R^2_{adj} = 0.65$). In Scots pine, latitude exerted a strong negative effect ($p < 0.001$), while elevation had a weaker but still significant influence ($p < 0.01$; $R^2_{adj} = 0.84$).

3.6. The effect of tree characteristics on the cessation of xylem cell enlargement

We examined model residuals to evaluate whether tree characteristics contributed to systematic prediction error. Tree diameter at breast height (DBH) and height showed significant positive relation with model residuals for Scots pine ($p < 0.01$, Fig. 5a). Notably, the total ring cell number (RCN) was also positively correlated with the model residuals in black spruce ($p < 0.01$), Norway spruce ($p = 0.05$) and Scots pine ($p = 0.1$, Fig. 5a, Supplementary Fig. 4). In contrast, tree age did not significantly affect residuals in any species (Fig. 5a). Beyond tree characteristics, the prediction error at the site-year level was significantly affected by the inter-tree variability in cE within each site-year. The model error (RMSE) was higher in site-years of higher inter-tree variability ($p < 0.01$, Fig. 5b).

4. Discussion

This study advances our understanding of phenological phases of wood formation in temperate coniferous species by identifying factors affecting the cessation of xylem cell enlargement (cE), which marks the end of stem radial growth. We examined the roles of temperature, photoperiod and soil moisture by developing three ecophysiological models that integrate these drivers. Among them, the *PiTs* model, which combines temperature and photoperiod, proved applicable across all three species. Overall, the *PiTs* model showed strong predictive accuracy, with a cross-species RMSE of 9.2 ± 1.3 days. This performance is consistent with the temporal resolution typically reported in xylogenesis monitoring studies, where the timing of cE is generally captured within a 7- to 14-day observational window.

4.1. Temperature and photoperiod control of cE

The *PiTs* model, supported by the majority of our data, emphasizes the critical roles of temperature and photoperiod in regulating cE across extensive geographical gradients. Previous research has demonstrated that low temperatures (approximately 10°C in experiments) are essential for controlling cambial activity and xylem cell differentiation (Begum et al., 2016; Begum et al., 2018; Gričar et al., 2006). Expanding on these findings, our results indicate that accumulated temperature plays a key role in driving cE. Although the fitted base temperature (*Tb*) in the *PiTs* model (24–30°C; Supplementary Fig. 2) appears relatively high, our critical values show strong agreement with leaf senescence models (25–29°C) (Archetti et al., 2013; Delpierre et al., 2009; Yang et al., 2012), providing a reference range in the absence of established thresholds. Furthermore, assessing the contributions of temperature ranges to the required temperature accumulation (*Ycrit*) revealed that accumulation is mainly driven by low-to-moderate temperatures, despite high fitted *Tb* (Supplementary Fig. 6). This dependence, amplified by the non-linear parameter (x = 2), highlights that "temperature decline", rather than absolute low temperature, is the primary driver of cE. Interestingly, the critical temperature sums estimated by the model are also consistent with those required to halt cambial activity in Gričar et al.'s stem-chilling experiments (the argument holds for Norway spruce, see Supplementary Fig. 5, Gričar et al., 2006), supporting the plausibility of our fitted thresholds. This broader understanding enhances our perspective on how temperature influences the cessation of wood formation.

Photoperiod signals the cessation of radial growth (Cuny et al., 2015; Saderi et al., 2019), a response that is particularly pronounced in trees at higher latitudes (Ekberg et al., 2010). In this study, we assumed that

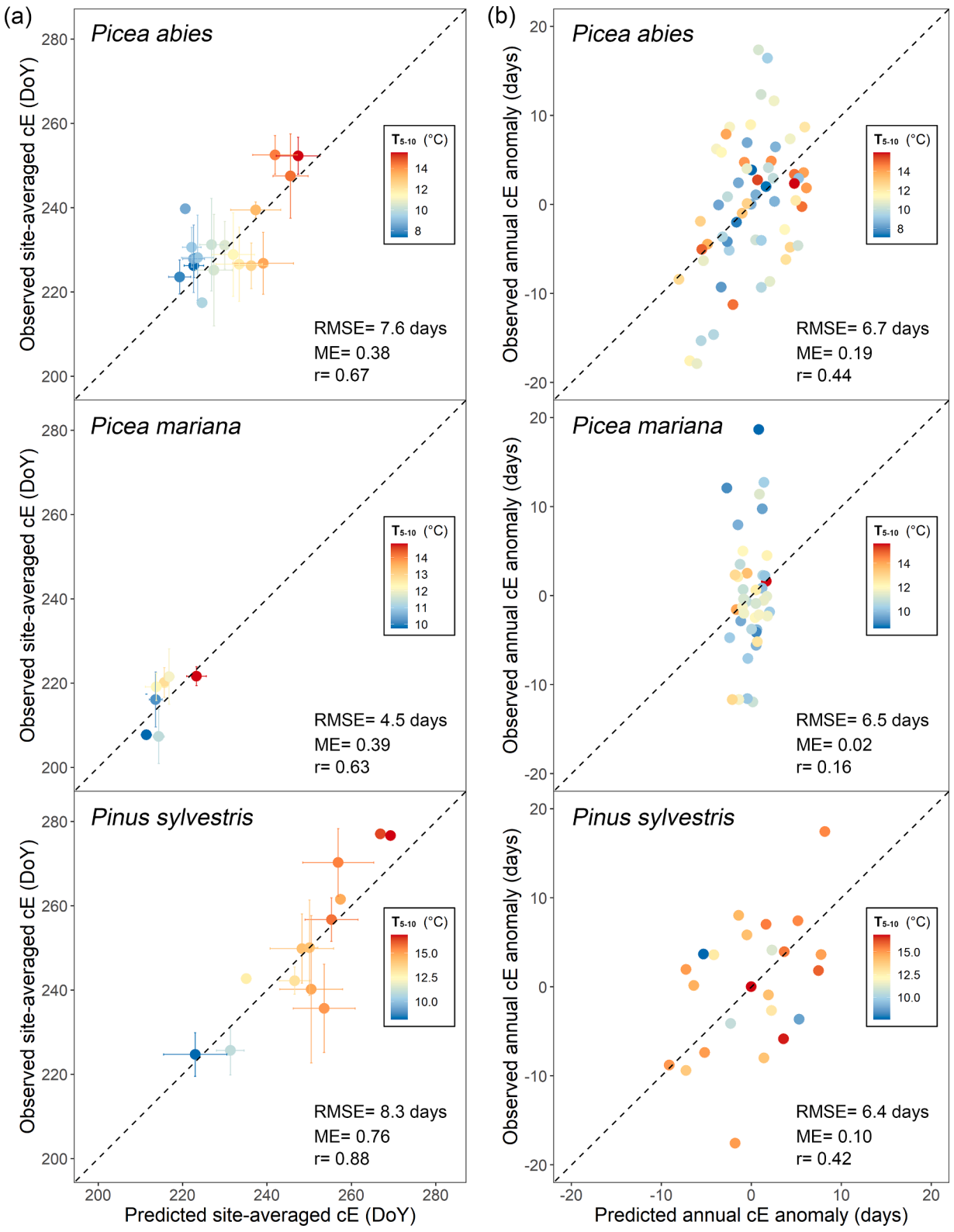

Fig. 3. Model evaluation for the cessation of xylem cell enlargement (cE) using the *PiTs* model in three Northern Hemisphere conifer species. (a) Model performance evaluated on validation data aggregated at the site level. Each point represents the mean predicted and observed cE date at a site; error bars indicate the standard deviation across years, reflecting interannual variability. (b) Model performance evaluated for annual anomalies at the site-year level. For calculating annual anomalies, we first aggregated the data at the site-year scale and then subtracted the average cE date, established along the observation period. In both panels, the one-to-one relationship is shown as a black dotted line. Model performance metrics include root mean square error (RMSE), correlation coefficient (r), and model efficiency (ME). Point colors represent mean temperature from May to October ($T_{5\text{-}10}$), either averaged per site (a) or per site-year (b).

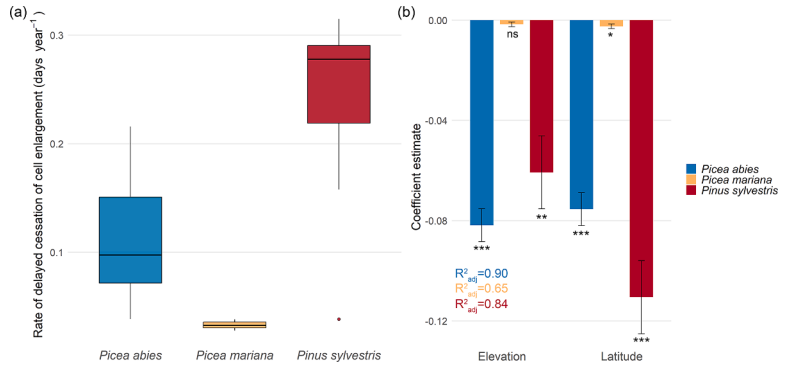

Fig. 4. Spatial variability in the temporal trend of the cessation of cell enlargement (cE) in relation to elevation and latitude for three Northern Hemisphere coniferous tree species. Plot (a) illustrates the temporal trend of cE across species, with error bars representing the standard deviation. Plot (b) illustrates the proportion of variance in the temporal trend explained by elevation and latitude for each species (adjusted R^2). Temporal trends were established over 1960 to 2023. Significance markers indicate whether elevation and latitude have a statistically significant linear effect on the delay rate. Elevation and latitude data were standardized using z-scores. ***: p<0.001, **: p<0.01, *: p<0.1, ns: p>0.1.

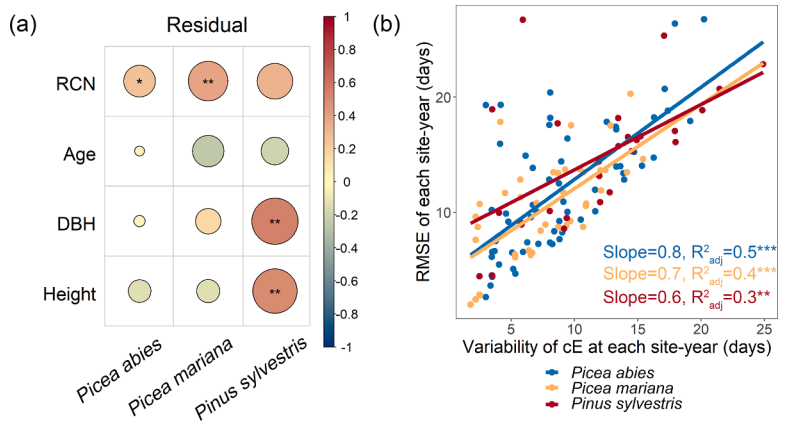

Fig. 5. The effect of intrinsic factors on the cessation of xylem cell enlargement (cE) for three Northern Hemisphere conifer species. Plot (a) is the correlation between the intrinsic factors (number of radial cell number (RCN), averaged at site-year scale; tree age, diameter at breast height (DBH) and height, averaged at site scale) and model residuals which were calculated as the difference between observed and predicted cE (using the *PiTs* model). The size of the dots and depth of color indicate the correlation coefficient. Plot (b) is the relation between variability of cE in the population (i.e. the inter-tree variability) and root mean square error (RMSE) for each site-year. One point represents one site-year. RMSE of each site-year was calculated based on predictions at the tree scale. Variability of cE is the standard deviation of cE, established across individual trees, in each site-year. ***: p<0.001, **: p<0.01, *: p<0.1.

photoperiod influences cE by modulating temperature accumulation, referencing previous models used for simulating leaf senescence (Archetti et al., 2013; Delpierre et al., 2009; Liu et al., 2019; Yang et al., 2012). Although temperature strongly influenced cE in all species (x = 2), incorporating photoperiod significantly improved model performance for Norway and black spruce (y = 1), but not for Scots pine (y = 0). This species-specific insensitivity aligns with experimental observations that Scots pine shoot growth ceases despite continued light exposure (Ekberg et al., 2010), and that its radial growth shows a weaker correlation with photoperiod compared to Norway spruce (Cuny et al., 2015).

4.2. Spatial variability and model limitations

The *PiTs* model robustly captured spatial variability in cE across the broad environmental gradient, reflecting geographic differences in temperature accumulation influenced by photoperiod (Supplementary Fig. 7). This performance suggests that environmental drivers dominate over local adaptation (Perrin et al., 2017). However, the model's limited ability to reproduce inter-annual variability highlights a challenge linked to our dataset structure. Characterized by high spatial but low temporal variance (3 ± 2 years per site), this dataset hampers the detection of temporal drivers (Buttò et al., 2020). We therefore tested whether incorporating soil moisture could resolve these unexplained inter-annual fluctuations. Contrary to expectations, this inclusion did not enhance model performance regardless of the integration window or depth. While Cabon et al. (2020) successfully linked inter-annual variations to water potential, a direct proxy for turgor pressure, our reliance on gridded soil moisture likely provided an incomplete representation of water stress. This limitation is particularly relevant in mountainous regions where gridded estimates lack precision, and at high-latitude sites, such as those in Canada (Buttò et al., 2020), that rarely experience significant moisture limitations. Consequently, although the *PiTs* model effectively captures the primary thermal and photoperiodic controls, future refinements should prioritize precise, site-specific water potential data to better resolve inter-annual dynamics.

4.3. Intrinsic constraints on prediction accuracy

Predicting the cessation of wood formation is inherently more challenging than its spring resumption due to multifactorial constraints (Cuny et al., 2019; Dox et al., 2020; Rossi et al., 2016). For example, the chilling-influenced heat-sum model predicts the beginning of cell enlargement (bE) with an accuracy better than 7 days (Delpierre et al., 2019), whereas the mean RMSE for cE in our study is 9.2 days. This lower accuracy reflects not only complex autumnal drivers but also the strong influence of intrinsic factors on growth cessation (Rathgeber et al., 2016; Rathgeber et al., 2011a). The total ring cell number (RCN),

which is influenced by both environmental factors and hormones, affects the timing of cE because producing more cells prolongs the enlargement period (Rossi et al., 2012). Consistent with this mechanism, all three species showed positive associations between RCN and model residuals. Tree size, particularly diameter at breast height (DBH) and height, also influenced residuals in the Scots pine, whereas no such effect was detected in the spruces. This pattern is consistent with the lack of consensus in previous studies, where some species show size-related extensions of the growing season (e.g., *Abies alba*; Rathgeber et al., 2011a) while others do not (e.g., *Juniperus przewalskii*; Zeng et al., 2017). Age had no significant effect across species ($p > 0.05$), consistent with Rossi et al. (2008), who reported similar cE timing across age classes in Norway spruce. These findings support our second hypothesis by demonstrating that tree-specific characteristics, particularly RCN, can influence cE, and thereby affect model accuracy.

Additionally, each site's RMSE increased with within-population variability in cE ($p < 0.05$), indicating that high population-level variability reduces prediction accuracy (Rathgeber et al., 2016). This also helps explain why cE is harder to model than bE, since cE exhibits markedly higher within-population variability (Supplementary Fig. 8). Finally, although observations followed a standardized protocol (Rathgeber et al., 2011b; Rossi et al., 2016), cE is inherently more difficult to determine than bE (Rathgeber et al., 2018), which lowers measurement precision and further contributes to reduced model performance. These results underscore the importance of incorporating intrinsic and environmental factors to enhance the predictive performance of cambium phenology models.

4.4. Physiological mechanisms underlying the model

The predictive success of the *PiTs* model likely stems from the fact that its environmental drivers, temperature and photoperiod, act as primary proxies for the complex physiological cascades regulating xylem differentiation. Current evidence indicates that these environmental cues act upstream of interconnected hormonal and metabolic pathways that ultimately suppress cambial activity. Specifically, shortening photoperiods and declining temperatures signal the down-regulation of auxin (IAA) and gibberellins (GAs), reducing the division potential of cambial initials and the enlargement capacity of differentiating xylem cells (Buttò et al., 2019; Eriksson et al., 2000; Immanen et al., 2016). Concomitantly, metabolic constraints arise as lower temperatures suppress the activity of key enzymes involved in cell-wall loosening and sucrose hydrolysis, thereby limiting turgor-driven expansion (Deslauriers et al., 2016; Immanen et al., 2016; Simard et al., 2013). Furthermore, seasonal shifts in carbohydrate allocation, characterized by the redirection of soluble sugars towards cold acclimation rather than structural growth, provide an additional carbon-based signal contributing to cessation (Simard et al., 2013). By integrating temperature and photoperiod, the *PiTs* model implicitly captures these coordinated physiological shutdowns, although explicitly incorporating such mechanistic links remains a frontier for improving model realism under future climate scenarios.

4.5. Warming-driven shifts in cE across regions and species

By incorporating photoperiod and temperature, our model successfully captures regional patterns of wood formation cessation. Using this framework to reconstruct cE over the past six decades, we found a widespread delay in cessation, with clear geographic variation that supports our third hypothesis. For Norway spruce and Scots pine, delay rates declined with increasing latitude and elevation, reflecting the limited capacity of trees in colder environments to extend the enlargement period (Rossi et al., 2006c; Rossi et al., 2011). In black spruce, the latitudinal pattern was weak and only marginally significant ($p < 0.1$), likely due to its narrower geographic range compared to the other species. Photoperiod further modulated these trends (Luo et al., 2018), as strong daylength constraints at high latitudes restricted the warming-driven delay in Norway spruce (Supplementary Fig. 7), while at low latitudes, longer early-autumn daylength slowed temperature accumulation and therefore postponed cE (Cuny et al., 2015; Jyske et al., 2014; Saderi et al., 2019). These results highlight the need to consider both geographic context and species-specific sensitivities when evaluating warming effects on wood formation.

5. Conclusion

Our study establishes the *PiTs* model as a robust ecophysiological framework for predicting cE in temperate conifers. We identified temperature decline, modulated by photoperiod, as the primary driver of growth cessation, revealing distinct species-specific sensitivities, particularly the lower photoperiodic responsiveness of Scots pine. By applying this model across extensive climate gradients, we quantified warming-induced delays in cessation, providing a scalable tool to enhance the realism of growing season dynamics in global carbon cycle models (Delpierre et al., 2016; Eckes-Shephard et al., 2022; Friend et al., 2019, 2022). While the model effectively captures spatial variability, challenges remain in reproducing inter-annual fluctuations, largely due to the limited temporal resolution of current datasets and the lack of site-specific water potential measurements. Future research should prioritize long-term monitoring to further refine these temporal dynamics and improve forest productivity simulations under climate change.

Data availability

The cessation of xylem cell enlargement data at site-year level used for model construction are provided in Supplementary Table 3. The raw wood formation data at the individual tree level are available upon reasonable request by contacting the corresponding author.

Code availability

The R codes used in this study are available at https://doi.org/10.5281/zenodo.15607017.

CRediT authorship contribution statement

Jianhong Lin: Conceptualization, Methodology, Formal analysis, Investigation, Writing – original draft. **Cyrille B.K. Rathgeber:** Conceptualization, Supervision, Methodology, Writing – review & editing. **Patrick Fonti:** Writing – review & editing. **Sergio Rossi:** Writing – review & editing. **Henri Cuny:** Writing – review & editing. **Edurne Martinez del Castillo:** Writing – review & editing. **Katarina Čufar:** Writing – review & editing. **J. Julio Camarero:** Writing – review & editing. **Alessio Giovannelli:** Writing – review & editing. **Harri Mäkinen:** Writing – review & editing. **Peter Prislan:** Writing – review & editing. **Walter Oberhuber:** Writing – review & editing. **Hanuš Vavrčík:** Writing – review & editing. **Jianguo Huang:** Writing – review & editing. **Andreas Gruber:** Writing – review & editing. **Vladimír Gryc:** Writing – review & editing. **Václav Treml:** Writing – review & editing. **Martin de Luis:** Writing – review & editing. **Jožica Gričar:** Writing – review & editing. **Nicolas Delpierre:** Conceptualization, Supervision, Methodology, Investigation, Writing – review & editing.

Declaration of competing interest

The authors declare that they have no known competing financial interests or personal relationships that could have appeared to influence the work reported in this paper.

Acknowledgements

This work was supported by the China Scholarship Council (202008330320). This research is a product of the FAIRWOOD project funded by the CESAB of the French Foundation for Research on Biodiversity (FRB). CBKR would like to thank the Agence Nationale de la Recherche (ANR) in the framework of the Investissements d'Avenir (ANR-11-LABX-0002-01, Laboratoire d'Excellence ARBRE) for the support given to its work as well as the SILVATECH platform (Silvatech, INRAE, 2018. Structural and functional analysis of tree and wood Facility, doi: 10.15454/1.5572400113627854E12) for its contribution to the acquisition of wood formation monitoring data. PF acknowledges support from the Swiss National Science Foundation project CALEIDOSCOPE (grant no. 212902). AG acknowledges support from the Austrian Science Fund (FWF P25643-B16 and P34706-B). AG acknowledges support from Provincia Autonoma di Trento (Project "SOFIE 2," 3012/2007). KČ, JG and PP acknowledge support from the Slovenian Research and Innovation Agency (ARIS), through programs P4-0015 (KČ), and P4-0430 (JG and PP). We further thank one anonymous reviewer for the constructive comments and suggestions that helped improve the paper.

Supplementary materials

Supplementary material associated with this article can be found, in the online version, at doi:10.1016/j.agrformet.2026.111056.

References

Aloni, R., 2013. Role of hormones in controlling vascular differentiation and the mechanism of lateral root initiation. Planta 238 (5), 819–830.
Archetti, M., Richardson, A.D., O'Keefe, J., Delpierre, N., 2013. Predicting climate change impacts on the amount and duration of autumn colors in a New England forest. PLoS One 8 (3), e57373.
Begum, S., et al., 2016. Localized cooling of stems induces latewood formation and cambial dormancy during seasons of active cambium in conifers. Ann. Bot. 117 (3), 465–477.
Begum, S., et al., 2018. Climate change and the regulation of wood formation in trees by temperature. Trees 32 (1), 3–15.
Burnham, K.P., Anderson, D.E., 2002. Model Selection And Multimodel Inference: A Practical Information-Theoretic Approach, 2nd ed. Springer-Verlag, New York.
Buttò, V., et al., 2019. The role of plant hormones in tree-ring formation. Trees 34 (2), 315–335.
Buttò, V., et al., 2020. Comparing the cell dynamics of tree-ring formation observed in microcores and as predicted by the Vaganov-Shashkin model. Front. Plant Sci. 11, 1268.
Cabon, A., Peters, R.L., Fonti, P., Martinez-Vilalta, J., De Caceres, M., 2020. Temperature and water potential co-limit stem cambial activity along a steep elevational gradient. New Phytol. 226 (5), 1325–1340.
Chen, Y., et al., 2022. Inter-annual and inter-species tree growth explained by phenology of xylogenesis. New Phytol. 235 (3), 939–952.
Corripio, J.G., 2019. insol: Solar Radiation (R package version 1.2.1).
Cuny, H.E., et al., 2019. Couplings in cell differentiation kinetics mitigate air temperature influence on conifer wood anatomy. Plant Cell Environ. 42 (4), 1222–1232.
Cuny, H.E., Rathgeber, C.B., 2016. Xylogenesis: coniferous trees of temperate forests are listening to the climate tale during the growing season but only remember the last words! Plant Physiol. 171 (1), 306–317.
Cuny, H.E., et al., 2015. Woody biomass production lags stem-girth increase by over one month in coniferous forests. Nat. Plants 1, 15160.
Delpierre, N., et al., 2009. Modelling interannual and spatial variability of leaf senescence for three deciduous tree species in France. Agric. For. Meteorol. 149 (6), 938–948.
Delpierre, N., et al., 2019. Chilling and forcing temperatures interact to predict the onset of wood formation in Northern Hemisphere conifers. Glob. Change Biol. 25 (3), 1089–1105.
Delpierre, N., et al., 2016. Temperate and boreal forest tree phenology: from organ-scale processes to terrestrial ecosystem models. Ann. For. Sci. 73 (1), 5–25.
Deslauriers, A., Huang, J.G., Balducci, L., Beaulieu, M., Rossi, S., 2016. The contribution of carbon and water in modulating wood formation in black spruce saplings. Plant Physiol. 170 (4), 2072–2084.
Deslauriers, A., Rossi, S., Anfodillo, T., Saracino, A., 2008. Cambial phenology, wood formation and temperature thresholds in two contrasting years at high altitude in southern Italy. Tree Physiol. 28 (6), 863–871.
Dox, I., et al., 2020. Timeline of autumn phenology in temperate deciduous trees. Tree Physiol. 40 (8), 1001–1013.
Dox, I., et al., 2022. Wood growth phenology and its relationship with leaf phenology in deciduous forest trees of the temperate zone of Western Europe. Agric. For. Meteorol. 327.
Eckes-Shephard, A.H., Ljungqvist, F.C., Drew, D.M., Rathgeber, C.B.K., Friend, A.D., 2022. Wood formation modeling – A research review and future perspectives. Front. Plant Sci. 13.
Ekberg, I., Eriksson, G., Dormling, I., 2010. Photoperiodic reactions in conifer species. Ecography 2 (4), 255–263.
Eriksson, M.E., Israelsson, M., Olsson, O., Moritz, T., 2000. Increased gibberellin biosynthesis in transgenic trees promotes growth, biomass production and xylem fiber length. Nat. Biotechnol. 18, 784–788.
Frieler, K., et al., 2017. Assessing the impacts of 1.5 °C global warming – simulation protocol of the inter-sectoral impact model intercomparison project (ISIMIP2b). Geosci. Model. Dev. 10 (12), 4321–4345.
Friend, A.D., Eckes-Shephard, A.H., Fonti, P., et al., 2019. On the need to consider wood formation processes in global vegetation models and a suggested approach. Ann. For. Sci. 76, 49. https://doi.org/10.1007/s13595-019-0819-x.
Friend, A.D., Eckes-Shephard, A.H., Tupker, Q., 2022. Wood structure explained by complex spatial source-sink interactions. Nat. Commun. 13 (1), 7824.
Gričar, J., Čufar, K., 2008. Seasonal dynamics of phloem and xylem formation in silver fir and Norway spruce as affected by drought. Russ. J. Plant Physiol. 55 (4), 538–543.
Gričar, J., Čufar, K., Oven, P., Schmitt, U., 2005. Differentiation of terminal latewood tracheids in silver fir trees during autumn. Ann. Bot. 95 (6), 959–965.
Gričar, J., et al., 2006. Effect of local heating and cooling on cambial activity and cell differentiation in the stem of Norway spruce (*Picea abies*). Ann. Bot. 97 (6), 943–951.
Hersbach, H., Bell, B., Berrisford, P., Biavati, G., Horányi, A., Muñoz Sabater, J., Nicolas, J., Peubey, C., Radu, R., Rozum, I., Schepers, D., Simmons, A., Soci, C., Dee, D., Thépaut, J-N., 2023. ERA5 hourly data on single levels from 1940 to present. Copernicus Climate Change Service (C3S) Climate Data Store (CDS).
Huang, J.G., et al., 2023. A critical thermal transition driving spring phenology of Northern Hemisphere conifers. Glob. Change Biol. 29 (6), 1606–1617.
Immanen, J., et al., 2016. Cytokinin and auxin display distinct but interconnected distribution and signaling profiles to stimulate cambial activity. Curr. Biol. 26 (15), 1990–1997.
Jackson, S.D., 2009. Plant responses to photoperiod. New Phytol. 181 (3), 517–531.
Jyske, T., Mäkinen, H., Kalliokoski, T., Nöjd, P., 2014. Intra-annual tracheid production of Norway spruce and Scots pine across a latitudinal gradient in Finland. Agric. For. Meteorol. 194, 241–254.
Liu, G., Chen, X., Fu, Y., Delpierre, N., 2019. Modelling leaf coloration dates over temperate China by considering effects of leafy season climate. Ecol. Modell. 394, 34–43.
Luo, T., et al., 2018. Summer solstice marks a seasonal shift in temperature sensitivity of stem growth and nitrogen-use efficiency in cold-limited forests. Agric. For. Meteorol. 248, 469–478.
Lupi, C., Morin, H., Deslauriers, A., Rossi, S., 2010. Xylem phenology and wood production: resolving the chicken-or-egg dilemma. Plant Cell Environ. 33 (10), 1721–1730.
Mu, W., et al., 2023. Photoperiod drives cessation of wood formation in northern conifers. Glob. Ecol. Biogeogr. 32, 603–617.
Muñoz Sabater, J. et al., 2024. ERA5-land post-processed daily-statistics from 1950 to present. Copernicus Climate Change Service (C3S) Climate Data Store (CDS).
Perrin, M., Rossi, S., Isabel, N., 2017. Synchronisms between bud and cambium phenology in black spruce: early-flushing provenances exhibit early xylem formation. Tree Physiol. 37 (5), 593–603.
Prislan, P., del Castillo, E.M., Skoberne, G., Špenko, N., Gričar, J., 2022. Sample preparation protocol for wood and phloem formation analyses. Dendrochronologia 73, 125959 (Verona).
R Core Team, 2023. R: A Language And Environment For Statistical Computing. R Foundation for Statistical Computing, Vienna, Austria.
Rathgeber, C.B.K., Cuny, H.E., Fonti, P., 2016. Biological basis of tree-ring formation: a crash course. Front. Plant Sci. 7, 734.
Rathgeber, C.B.K., Rossi, S., Bontemps, J.D., 2011a. Cambial activity related to tree size in a mature silver-fir plantation. Ann. Bot. 108 (3), 429–438.
Rathgeber, C.B.K., Longuetaud, F., Mothe, F., Cuny, H., Le Moguédec, G., 2011b. Phenology of wood formation: data processing, analysis and visualisation using R (package CAVIAR). Dendrochronologia 29 (3), 139–149 (Verona).
Rathgeber, C.B.K., Santenoise, P., Cuny, H.E., 2018. CAVIAR: an R package for checking, displaying and processing wood-formation-monitoring data. Tree Physiol. 38 (8), 1246–1260.
Rossi, S., et al., 2016. Pattern of xylem phenology in conifers of cold ecosystems at the Northern Hemisphere. Glob. Change Biol. 22 (11), 3804–3813.
Rossi, S., Anfodillo, T., Menardi, R., 2006a. Trephor: a new tool for sampling microcores from tree stems. IAWA J. 27, 89–97.
Rossi, S., Deslauriers, A., Anfodillo, T., 2006b. Assessment of cambial activity and xylogenesis by microsampling tree species: an example at the alpine timberline. IAWA J. 27 (4), 383–394.
Rossi, S., Deslauriers, A., Anfodillo, T., Carrer, M., 2008. Age-dependent xylogenesis in timberline conifers. New Phytol. 177 (1), 199–208.
Rossi, S., et al., 2006c. Conifers in cold environments synchronize maximum growth rate of tree-ring formation with day length. New Phytol. 170 (2), 301–310.
Rossi, S., Morin, H., Deslauriers, A., 2012. Causes and correlations in cambium phenology: towards an integrated framework of xylogenesis. J. Exp. Bot. 63 (5), 2117–2126.
Rossi, S., Morin, H., Deslauriers, A., Plourde, P.Y., 2011. Predicting xylem phenology in black spruce under climate warming. Glob. Change Biol. 17 (1), 614–625.

Saderi, S., Rathgeber, C.B.K., Rozenberg, P., Fournier, M., 2019. Phenology of wood formation in larch (*Larix decidua* Mill.) trees growing along a 1000-m elevation gradient in the French Southern Alps. Ann. For. Sci. 76 (3), 89.
Schrader, J., et al., 2003. Polar auxin transport in the wood-forming tissues of hybrid aspen is under simultaneous control of developmental and environmental signals. Proc. Natl. Acad. Sci. U. S. A. 100 (17), 10096–10101.
Simard, S., et al., 2013. Intra-annual dynamics of non-structural carbohydrates in the cambium of mature conifer trees reflects radial growth demands. Tree Physiol. 33 (9), 913–923.
Traversari, S., et al., 2018. Can sugar metabolism in the cambial region explain the water deficit tolerance in poplar? J. Exp. Bot. 69 (16), 4083–4097.
Tumajer, J., et al., 2021. Forward modeling reveals multidecadal trends in cambial kinetics and phenology at treeline. Front. Plant Sci. 12, 613643.
Wei, T. and Simko, V., 2021. R package 'corrplot': Visualization of a correlation matrix (Version 0.92).
Wu, C., et al., 2022. Increased drought effects on the phenology of autumn leaf senescence. Nat. Clim. Change 12 (10), 943–949.
Yang, X., Mustard, J.F., Tang, J., Xu, H., 2012. Regional-scale phenology modeling based on meteorological records and remote sensing observations. J. Geophys. Res. Biogeosciences 117 (G3).
Zeng, Q., Rossi, S., Yang, B., 2017. Effects of age and size on xylem phenology in two conifers of northwestern China. Front. Plant Sci. 8, 2264.